IEEE Access
Multidisciplinary ⋮ Rapid Review ⋮ Open Access Journal

Received August 10, 2020, accepted August 26, 2020, date of publication September 10, 2020, date of current version September 23, 2020.

Digital Object Identifier 10.1109/ACCESS.2020.3023136

A Framework of Multipath Mitigation With Joint Multipath-Doppler Diversity for RF Relative Measurement

WEIQING MU[1], ZIJIE WANG[2], LANTU GUO[3], AND YANAN LIU[4]

[1]China Research Institute of Radiowave Propagation, Qingdao 266107, China
[2]School of Electronic and Information Engineering, Beihang University, Beijing 100191, China
[3]School of Information and Electronics, Beijing Institute of Technology, Beijing 100081, China
[4]School of Information and Communication Engineering, Harbin Engineering University, Harbin 150001, China

Corresponding authors: Weiqing Mu (weiqing0017@163.com) and Lantu Guo (guolantu@163.com)

This work was supported in part by the National Natural Science Foundation of China under Grant 91438116, and in part by the Program for New Century Excellent Talents under Grant NCET-12-0030.

ABSTRACT Radio frequency (RF) relative measurement provides an effective means of communication and autonomous navigation for the spacecraft formation flying. Multipath and Doppler are two main factors that affect the accuracy of RF relative measurement. In this study, a framework that exploits joint multipath-Doppler diversity is proposed to reduce multipath errors and improve the measurement accuracy. The proposed framework first utilizes an Extended Kalman Filter (EKF) estimator to estimate the parameters of Doppler and multipath. Different from existing research, the proposed framework reconstructs the received signal according to the estimated parameters, so as to mitigate multipath signals and enhance the direct signal. Numerical results demonstrate that the framework is suitable for both multipath and multipath-Doppler scenarios, and has a significant performance improvement over existing multipath mitigation methods.

INDEX TERMS Multipath mitigation, multipath-Doppler, RF relative measurement, EKF estimation.

I. INTRODUCTION

One distinctive showcase of a distributed space system (DSS) is known as spacecraft formation flying [1]. Radio Frequency (RF) measurement presents a relative navigation solution that can be of interest to the earth-orbiting satellites. It also provides a way for communication and network of satellites in the group [2]. Accurate relative navigation between satellites can be executed by onboard embedded systems with RF relative measurement abilities. Using the onboard embedded system to perform relative measurement has various benefits for satellite formation flying. On the one hand, relative measurement could be used to enhance the accuracy achieved by Global Navigation Satellite System (GNSS). On the other hand, RF relative measurement provides an alternative solution for relative navigation in deep space where GNSS is unavailable [3]. Numerous missions with high-accuracy demands on the inter-spacecraft position have been flown or proposed. National Aeronautics and Space Administration has developed the Autonomous Formation Flying (AFF) technology for many missions (StarLight/DS3/ST3) [4]–[6]. Formation Flying Radio Frequency (FFRF) sensor is another RF-based technology developed by the National Center for the PRISMA mission [3], [7].

In spacecraft formation flying scenarios where multiple spacecrafts utilizes inter-spacecraft links to transmit signals and perform relative measurement, signals are likely to be reflected on the surface of spacecrafts. Some reflections may occasionally come from a third close-by spacecraft in the formation, or from the spacecraft's body, such as solar panels [8], but generally within a short time duration. Especially, RF measurement sensors are used for space station rendezvous and docking. When the space station and the spacecraft are in relative motion, and between the direct signal and multipath signal there is a relative velocity, thence, a relative Doppler shift is generated between the both. Therefore, in this case there is a carrier frequency difference between the multipath and direct signal, that is, the multipath-Doppler described in this study.

The existing multipath mitigation methods mainly include: the narrow correlator (NC) [9], the strobe correlator [10], the multipath estimating delay lock loop

The associate editor coordinating the review of this manuscript and approving it for publication was Zhaojun Li.

method (MEDLL) [11], the multi-antenna multipath estimation method [12]. However, the methods proposed in [10] and [11], to a certain extent, mitigate multipath on delay lock loop (DLL), but cannot completely eliminate multipath errors, especially in the presence of the short delays multipath, the DLL's tracking range will be reduced. As [11] point out MEDLL is proposed based on the maximum likelihood theory. This technique is computational expensive [13], [14]. The method proposed in [12] is a tool of multipath mitigation by utilizing the geometrical relationship of multiple antennas, and thus requires the addition of hardware equipment, is not applicable to this study. Moreover, these methods do not take into account the carrier frequency difference between the multipath signal and the direct signal, thus it cannot accurately estimate multipath parameters when the multipath-Doppler is present.

It's worth noting that in most existing research, multipath signals are considered as undesirable signals and are eliminated from the received signal [19], [20]. Different from the above methods, [15] presented a novel method in which the signals are used to reconstruct the received signals instead of being eliminated. However, this method do not enhance the direct signal, even the correlation peak is reduced in the presence of the multipath-Doppler.

Aiming at the shortcomings of the existing methods, in this study a promising framework of multipath mitigate is proposed for space applications where multipath or multipath-Doppler is existed, in which Doppler and multipath parameters are accurately estimated by an EKF estimator, and then the received signal is reconstruct based on the joint multipath-Doppler diversity. Therefore, the multipath error is mitigated and the direct signal is enhanced in present of multipath-Doppler; in addition, the proposed framework is still valid for scenes with only multipath.

The organization of the study is as follows: Section 2 describes RF relative measurement model and presents multipath-Doppler; Section 3 analyzes multipath and multipath-Doppler in code tracking loop; Section 4 presents a framework of multipath mitigation based on the joint multipath-Doppler diversity; results of experiments are shown in Section 5, and finally we conclude the study in Section 6.

II. THEMULTIPATH AND MULTIPATH-DOPPLER IN RF RELATIVE MEASUREMENT

A. RF RELATIVE MEASUREMENT MODEL

The RF relative measurement between spacecrafts is a compelling technology in the space mission aimed at detecting, acquiring, and tracking the relative position and attitude between spacecrafts. The application of RF relative measurement technology provides an effective relative navigation and control method for low-earth-orbit (LEO) spacecrafts whose visibility of GNSS constellation is limited and spacecrafts at altitudes above the GNSS constellations. RF relative measurement system is shown in Fig. 1, enabling a joint inter-spacecraft communication and relative navigation.

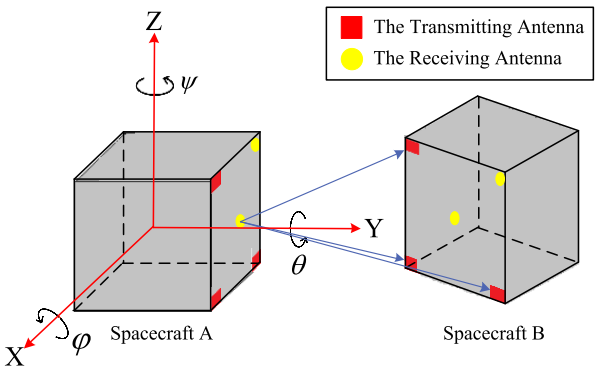

FIGURE 1. RF relative measurement system.

There are two types of antennas on each spacecraft in the RF relative measurement system, that is, two transmitting antennas and three receiving antennas. Each transmitting antenna generates and transmits GNSS-like RF ranging signal, and the multiple access of multiple signals from different transmitting antennas employ Code Division Multiple Access (CDMA). At any measurement epoch, a ranging observation can be measured between any transmitting antenna and any receiving antenna on a different spacecraft. Therefore, for the RF relative measurement system, 12 ranging observations as shown in Eq.1 can be obtained at each measurement epoch.

$$\rho = \left[\rho_{A_1b_1}, \rho_{A_1b_1}, \rho_{A_1b_1}, \rho_{A_2b_1} \cdots \rho_{B_2a_3}\right] \tag{1}$$

where $\rho_{A_1b_1}$ is the ranging observation measured between the i-th transmitting antenna of spacecraft A and the j-th receiving antenna of spacecraft B. The capital letters A and B represent the transmitting antennas on spacecraft A and spacecraft B, respectively, while lowercase letters a and b represent the receiving antennas. The ranging model is given by:

$$\rho_{A_ib_j} = \sqrt{r_{A_ib_j} r^T_{A_ib_j}} + c\Delta\tau \tag{2}$$

where Vτ is the clock error between two spacecrafts; c is the velocity of light; $r_{A_ib_j}$ is the vector from i-th transmitting antenna of spacecraft A to the j-th receiving antenna of spacecraft B and can be expressed as:

$$\begin{aligned} r_{A_ib_j} = {} & [d\cos\alpha\cos\gamma, d\cos\alpha\sin\gamma, d\sin\alpha] \\ & + \left[Q(\varphi_B, \theta_B, \psi_B)\, u_{b_j} - Q(\varphi_A, \theta_A, \psi_A)\, u_{A_i}\right] \end{aligned} \tag{3}$$

where d is the relative distance of two spacecrafts; α and γ are the relative elevation angle and azimuth angle of two spacecrafts, respectively; u_{A_i} is the location of i-th transmitting antenna in the local co-rotating Cartesian frame of spacecraft A. φ_A, θ_A and ψ_A are the rotation angles of spacecraft A with respect to the reference frame, as shown in the Fig.1. For convenience, the local co-rotation Cartesian frame of spacecraft A is set as the reference frame of the whole system, so that $\varphi_A = 0°$, $\theta_A = 0°$, $\psi_A = 0°$, and $\varphi_B, \theta_B, \psi_B$ are the

relative rotation angles of two spacecrafts; $Q(\cdot)$ is the rotation matrix corresponding to rotation angles.

The Least Square algorithm or EKF can be employed to solve the ranging equations, and the estimates of relative position and attitude can be obtained as follows:

$$X = [d, \alpha, \gamma, \varphi_B, \theta_B, \psi_B, \Delta\tau] \tag{4}$$

B. MULTIPATH-DOPPLER IN RF RELATIVE MEASUREMENT

During RF relative measurement between spacecrafts, the measurement signal may be degraded by multipath signals being reflected by the spacecraft itself or other spacecrafts operating nearby. In addition, in the case of distance between spacecrafts is small, such as the rendezvous and docking of spacecrafts, multipath signals can cause large ranging errors in the receiver at ranges below a few hundred meters. This kind of ranging error caused by multipath signals makes the RF relative measurement system incorrectly determine the relative position and attitude of spacecrafts, and seriously affect the operation of the spacecrafts. The existing researches show that the solar array panel on the spacecraft is one of the main reasons for the reflection of the measurement signal. Figure 2 shows an example of multipath signal reflected by the solar array panel of the International Space Station (ISS) in the scenario of rendezvous and docking of a spacecraft and the ISS [8], [18].

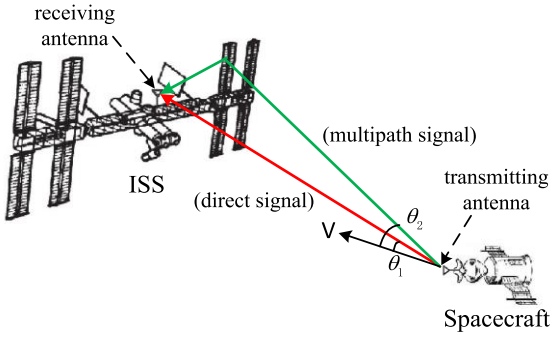

FIGURE 2. Multipath and Doppler in rendezvous and docking scenario.

The red line in Fig.2 is the direct signal from the spacecraft, and the green line is the multipath signal. θ_1 is the angle between the relative velocity vector and the direct signal, and θ_2 is the angle between the relative velocity vector and the multipath signal [18].

It is worth noting that the Doppler and multipath can be observed in the signal received by the receiver due to the relative motion of the spacecrafts during the RF relative measurement [16], [17]. Moreover, when the projection of the relative velocity vector in the direction of the direct signal is not the same as the projection in the direction of the multipath signal, the instantaneous Doppler shift of the multipath signal received by the receiver can be significantly different from the direct signal. Taking the scenario shown in Fig. 2 as an example, the Doppler shift of the direct signal received by the ISS receiving antenna compared to the multipath signal (in units of Hz) is given by:

$$\Delta f_d = \frac{|V|\,(\cos(\theta_1) - \cos(\theta_2))}{\lambda} \tag{5}$$

where V is the relative velocity vector between spacecraft and ISS, and λ is the wavelength of the measurement signal.

To improve the precision of ranging to satisfy the requirements of attitude estimation, the carrier frequency of the measurement signal used in this study is increased compared with that used in PRISMA [3], [7]. Considering ranging accuracy and other factors comprehensively, the carrier frequency of the RF relative measurement system is set to Ku band (10GHz or so). When the rendezvous and docking is operated in the final stage, the relative velocity is approximately 1-3m/s. The angles between relative velocity vector and direct signal and multipath signal are $\theta_1 = 5°$ and $\theta_2 = 45°$, respectively, the Doppler shift difference between the direct signal and multipath signal can reach approximately 30 Hz.

From the above analysis, it can be concluded that the multipath can occur during the relative measurement between the spacecrafts, and the Doppler shift of the multipath signal can be different from the direct signal. In this study this is described as multipath-Doppler.

III. MULTIPATH AND MULTIPATH-DOPPLER IN CODE TRACKING LOOP

The ranging signal architecture of RF relative measurement adopted in this study is GNSS-like signal architecture. Compared to other signal architecture (UWB, FMCW, etc.), GNSS-like ranging signal architecture has the highest technical maturity and takes full advantages of experiences on GNSS hardware and software in space applications [18]. In this study, a novel multipath mitigation framework is proposed. This framework can make full use of joint multipath-Doppler diversity, and increase the intensity of direct signals in the presence of the multipath-Doppler. At the same time this method can be compatible with multipath scenarios. Therefore, the signal analysis is carried out from both the multipath scenario and the multipath-Doppler scenario.

A. MULTIPATH OF RANGING SIGNAL

In the RF relative measurement, a sampled GNSS-like Intermediate Frequency (IF) ranging signal received by a single direct path can be written as follows:

$$r_d(kT_s) = Ac(kT_s - \varepsilon)\cos((\omega_{IF} + \omega_d)kT_s + \theta_d) + n(kT_s) \tag{6}$$

where A is amplitude of the sampled IF signal (V); $c(\cdot)$ is the PRN code in the GNSS-like ranging signal; $\cos((\omega_{IF} + \omega_d)kT_s + \theta)$ is the sampled IF carrier; T_s is the sampling period (s); ω_{IF} is the IF frequency down-converted from the radio frequency (rad/s); ω_d is the Doppler shift of the sampled IF signal (rad/s); θ_d is the initial phase of IF carrier (rad); $n(kT_s)$ is the noise.

Following the usual signal flow in a RF measurement receiver, the sampled IF signal $r_d(kT_s)$ is input to a coherent

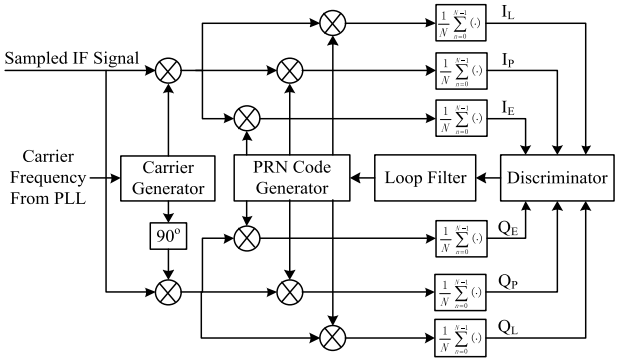

FIGURE 3. Coherent delay lock loop.

DLL shown in Fig.3. In DLL the incoming IF signal is mixed with the locally generated in-phase and quadrature-phase replicas of the carrier. After that, the signal is correlated with the early (E), prompt (P) and late (L) versions of the locally generated PRN code, and the correlation values are integrated for a certain integration period. The local in-phase prompt signal combining the code and carrier generated by the local PRN code generator and carrier generator can be expressed as:

$$S_{I_P}(kT_s) = c(kT_s - \hat{\varepsilon})\cos((\omega_{IF}+\hat{\omega})kT_s+\hat{\theta}) \tag{7}$$

where $\hat{\varepsilon}$ is the estimate of the received signal code delay (s); $\hat{\omega}$ is the estimate of the received signal Doppler shift (rad/s); $\hat{\theta}$ is the estimate of the received signal initial carrier phase (rad). Without loss of generality, assuming that the Doppler shift of received signal and its estimate are the same, that is, $\omega_d = \hat{\omega}$. Then, the in-phase prompt correlation value is given by:

$$\begin{aligned} I_P &= \sum_{k=k_{0,j}}^{k_{0,j}+N-1} r_d(kT_s)S_{I_P}(kT_s) \\ &\approx \frac{AT_j}{2T_s}R(\mathrm{V}\varepsilon)\cos(\mathrm{V}\theta_d) \end{aligned} \tag{8}$$

where $k_{0,j}$ is the sample point at which the j-th integration begins; N is the number of sample points to be integrated; T_j is the integration time corresponding to N sampling points. $R(\cdot)$ is the auto-correlation function of the PRN code; $\mathrm{V}\varepsilon = \varepsilon - \hat{\varepsilon}, \mathrm{V}\theta_d = \theta_d - \hat{\theta}$. Similarly, the in-phase early (I_E), in-phase late (I_L), quadrature-phase prompt (Q_P), quadrature-phase early (Q_E) and quadrature-phase late (Q_L) correlation values can be expressed respectively as:

$$I_E = \frac{AT_j}{2T_s}R(\mathrm{V}\varepsilon - \mathrm{V}\tau)\cos(\mathrm{V}\theta_d) \tag{9}$$

$$I_L = \frac{AT_j}{2T_s}R(\mathrm{V}\varepsilon + \mathrm{V}\tau)\cos(\mathrm{V}\theta_d) \tag{10}$$

$$Q_P = \frac{AT_j}{2T_s}R(\mathrm{V}\varepsilon)\sin(\mathrm{V}\theta_d) \tag{11}$$

$$Q_E = \frac{AT_j}{2T_s}R(\mathrm{V}\varepsilon - \mathrm{V}\tau)\sin(\mathrm{V}\theta_d) \tag{12}$$

$$Q_L = \frac{AT_j}{2T_s}R(\mathrm{V}\varepsilon + \mathrm{V}\tau)\sin(\mathrm{V}\theta_d) \tag{13}$$

where $\mathrm{V}\tau$ is the spacing in chips between the prompt and early, or the prompt and late code. A coherent early-minus-late (CELP) discriminator is used for code tracking in this study. Assuming that the frequency and phase of locally generated carrier are the same as the frequency and phase of received carrier, the discriminator function is given by:

$$\begin{aligned} D_c &= I_E - I_L \\ &= \frac{AT_j}{2T_s}\left[R(\mathrm{V}\varepsilon - \mathrm{V}\tau) - R(\mathrm{V}\varepsilon + \mathrm{V}\tau)\right] \end{aligned} \tag{14}$$

In the presence of multipath, the sampled IF signal consists of a direct signal and M multipath signal can be expressed as:

$$\begin{aligned} r_{cm}(kT_s) &= r_d(kT_s) + \sum_{i=1}^{M} r_{m_i}(kT_s) + n(kT_s) \\ &= Ac(kT_s - \varepsilon)\cos((\omega_{IF}+\omega_d)kT_s+\theta_d) \\ &\quad + A\sum_{i=1}^{M}\alpha_i c(kT_s - \varepsilon - l_i)\cos((\omega_{IF}+\omega_d)kT_s+\theta_i) \\ &\quad + n(kT_s) \end{aligned} \tag{15}$$

where $r_{m_i}(kT_s)$ is the sampled IF signal received by i-th reflect path, that is, i-th multipath signal. α_i is the relative amplitude coefficient between the direct signal and the i-th multipath signal. l_i is the time-delay between the direct signal and the i-th multipath signal, and must be positive given in the convention used in the Eq.13. θ_i is the initial carrier phase of the i-th multipath signal. With this new received IF signal, assuming that the frequency of direct signal and the frequency of locally generated carrier are the same ($\hat{\omega} = \omega_d$), the output of correlator becomes:

$$I_P = \frac{AT_j}{2T_s}R(\mathrm{V}\varepsilon)\cos(\mathrm{V}\theta_d) + \frac{AT_j}{2T_s}\sum_{i=1}^{M}\alpha_i R(\mathrm{V}\varepsilon + l_i)\cos(\mathrm{V}\theta_i) \tag{16}$$

where $\mathrm{V}\theta_i = \theta_i - \hat{\theta}$. Assuming that the frequency and phase of locally generated carrier are the same as that of the direct signal's carrier, the output of discriminator becomes:

$$\begin{aligned} D_c &= \frac{AT_j}{2T_s}\left[R(\mathrm{V}\varepsilon - \mathrm{V}\tau) - R(\mathrm{V}\varepsilon + \mathrm{V}\tau)\right] \\ &\quad + \frac{AT_j}{2T_s}\sum_{i=1}^{M}\left[R(\mathrm{V}\varepsilon + l_i - \mathrm{V}\tau) - R(\mathrm{V}\varepsilon + l_i + \mathrm{V}\tau)\right] \\ &\quad * \cos(\theta_i - \theta_d) \end{aligned} \tag{17}$$

Therefore, Eqs.16 and 17 are respectively the correlation function and the discriminator function, based on this the curves of the both can be drawn. Figs.4 and 5 show the correlation function and discriminator function for the received signal containing a single multipath signal respectively, when $\mathrm{V}\theta_d = 0$, $\alpha_1 = 0.5$, $l_1 = 0.5\,(chips)$, $\mathrm{V}\theta_1 = 0°or180°$. It is clear that the correlation function of the received signal is distorted due to the presence of multipath, and the zero-crossing point of the discriminator function is no longer at $\mathrm{V}\varepsilon = 0$. Since the DLL tracks the code phase of input signal by tracking the zero-crossing point of the discriminator

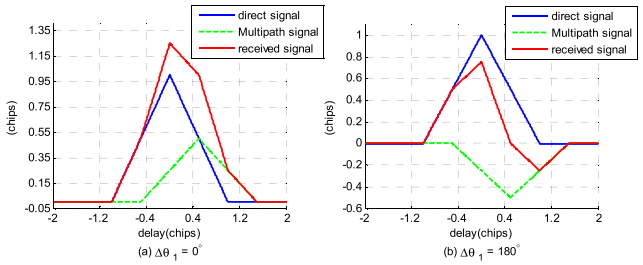

FIGURE 4. The curve of correlation function.

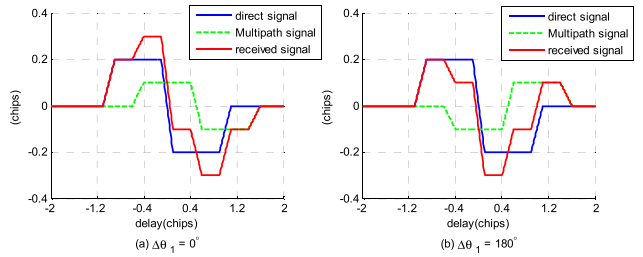

FIGURE 5. The discriminator curve.

function, the code tracking result output by DLL contains a remaining bias due to multipath. This bias between the point $V\varepsilon = 0$ and the zero-crossing point of the discriminator function is defined as multipath error.

Multipath error envelope is a common and recognized way to analyze the multipath, and it's definition is the multipath errors corresponding to all the potential multipath delays from 0 to 1.5 chips with a given relative amplitude coefficient.

The upper and lower bounds of multipath error envelope is defined when $V\theta_1 = 0°$ and $V\theta_1 = 180°$, respectively. When $\alpha_1 = 0.5$, $V\tau = 0.1$ (*chips*), multipath error envelop is shown in Fig.6.

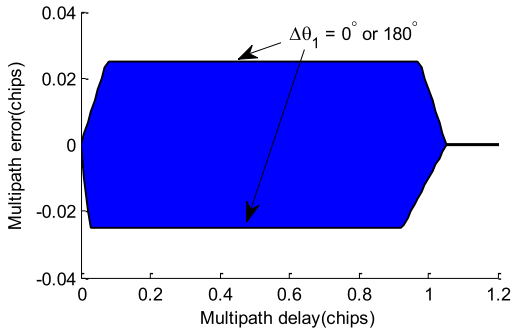

FIGURE 6. Multipath error envelop.

B. MULTIPATH-DOPPLER OF RANGING SIGNAL

For the purpose of getting the difference between multipath-Doppler and multipath. It is also discussed from the following three aspects as multipath, that is, correlation function, discriminator function, and multipath error envelope.

In the presence of multipath-Doppler, the sampled IF signal consists of a direct signal and M multipath signal can be expressed as:

$$\begin{aligned} r_{cmd}(kT_s) &= r_d(kT_s)+\sum_{i=1}^{M} r_{md_i}(kT_s)+n(kT_s) \\ &= Ac(kT_s-\varepsilon)\cos((\omega_{IF}+\omega_d)kT_s+\theta_d) \\ &\quad +A\sum_{i=1}^{M}\alpha_i c(kT_s-\varepsilon-l_i) \\ &\quad *\cos((\omega_{IF}+\omega_d-V\omega_{m_i})kT_s+\theta_i)+n(kT_s) \end{aligned} \tag{18}$$

where $r_{md_i}(kT_s)$ is the sampled IF signal received by i-th reflect path whose Doppler shift is different from the Doppler shift of the direct signal, that is, i-th multipath-Doppler signal; $V\omega_{m_i}$ is the Doppler shift of the direct signal compared to the i-th multipath-Doppler signal.

Assuming that the frequency of direct signal and the frequency of locally generated carrier are the same ($\hat{\omega} = \omega_d$), the output of correlator can be derived as follows:

$$\begin{aligned} I_P &= \sum_{k=k_{0,j}}^{k_{0,j}+N-1} r_{cmd}(kT_s)S_{I_p}(kT_s) \\ &= \sum_{k=k_{0,j}}^{k_{0,j}+N-1} \frac{A}{2} \\ &\quad \left[\begin{array}{l} c(kT_s-\varepsilon)c\left(kT_s-\hat{\varepsilon}\right)\cos(V\theta_d) \\ +\sum_{i=1}^{M}\alpha_i c(kT_s-\varepsilon-l_i)c(kT_s-\hat{\varepsilon})\cos(-V\omega_{m_i}kT_s+V\theta_i) \end{array}\right] \\ &\approx \frac{A}{2T_s}\int_{T_{0,j}}^{T_{0,j}+T_j} c(kT_s-\varepsilon)c(kT_s-\hat{\varepsilon})\cos(V\theta_d)dt \\ &\quad +\frac{A}{2T_s}\sum_{i=1}^{M}\left[\alpha_i\int_{T_{0,j}}^{T_{0,j}+T_j} c(kT_s-\varepsilon-l_i)c(kT_s-\hat{\varepsilon})\right. \\ &\quad \left.\cos(-V\omega_{m_i}kT_s+V\theta_i)dt\right] \\ &\approx \frac{AT_j}{2T_s}R(V\varepsilon)\cos(V\theta_d) \\ &\quad +\sum_{i=1}^{M}\frac{AT_j}{2T_s}R(V\varepsilon+l_i)\sin c(-V\omega_{m_i}T_j/2)\cos(V\phi_{i,j}) \end{aligned} \tag{19}$$

where $T_{0,j}$ is start time of the j-th integration, and $V\phi_{i,j} = -V\omega_{m_i}(T_{0,j}+T_j/2)+V\theta_i$. Since $\sin c(V\omega_{m_i}T_j/2) \approx 1$, when $V\omega_{m_i}T_j/2 \ll 1$, the output of correlator can be expressed as:

$$I_P = \frac{AT_j}{2T_s}R(V\varepsilon)\cos(V\theta_d)+\frac{AT_j}{2T_s}\sum_{i=1}^{M}\alpha_i R(V\varepsilon+l_i)\cos(V\phi_{i,j}) \tag{20}$$

In addition, the output of CELP discriminator function in the presence of multipath-Doppler becomes:

$$\begin{aligned} D_c &= \frac{AT_j}{2T_s}[R(V\varepsilon-V\tau)-R(V\varepsilon+V\tau)] \\ &\quad +\frac{AT_j}{2T_s}\sum_{i=1}^{M}[R(V\varepsilon+l_i-V\tau)-R(V\varepsilon+l_i+V\tau)]\cos(V\phi_{i,j}) \end{aligned} \tag{21}$$

Note that $V\phi_{i,j}$ change over time (number of integration) in the presence of multipath-Doppler, thus the outputs of the correlator and discriminator are both the functions of time. This is the most significant difference compared to the normal multipath in code tracking.

Moreover, a more effective and intuitive way to analyze the time-variant characteristics of multipath-Doppler is to study the variation of multipath error with time. Figure 7 shows the multipath error envelopes of a received signal at four different moments in the presence of the Multipath-Doppler, where the received signal consists of a direct signal and a single multipath-Doppler signal. The Doppler of the direct signal compared to the multipath signal is 25Hz (157rad/s).

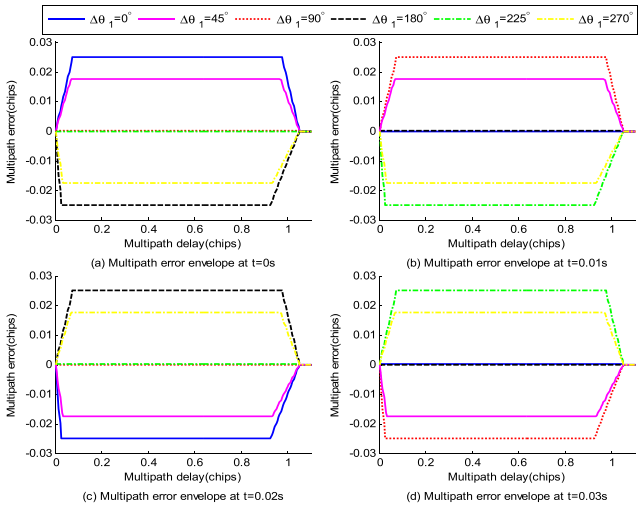

FIGURE 7. Multipath error envelopes with time.

Figure 7 shows multipath error envelopes at different moment. The upper and lower bounds look the same as those in Fig.6 which is only present of multipath. However, the multipath error curve corresponding to a specific initial carrier phase difference ($V\theta_1$) changes with time. Therefore, the multipath error curve with time is simulated and restored, and then produced the surface of multipath error. Figure 8 shows the surface of multipath error formed by the variation of the multipath error curve corresponding to $V\theta_1 = 0°$ with time.

In Fig.8 the pink pattern is the projection of the multipath error surface on the multipath delay-multipath error plane, and the blue pattern is the projection of the multipath error surface on the time-multipath error plane. It is clear that, the shape of the pink pattern is the same as the shape of the multipath error envelope in Fig.7, and the shape of the blue pattern has a sinusoidal feature with time. Thus, it can be concluded that the multipath error corresponding to a specific initial carrier phase difference $V\theta_1$ and multipath delay l_1 changes periodically in a sinusoidal form within the multipath error envelope over time.

As analyzed in this section, in the presence of multipath-Doppler, there are time-varying multipath errors in the output

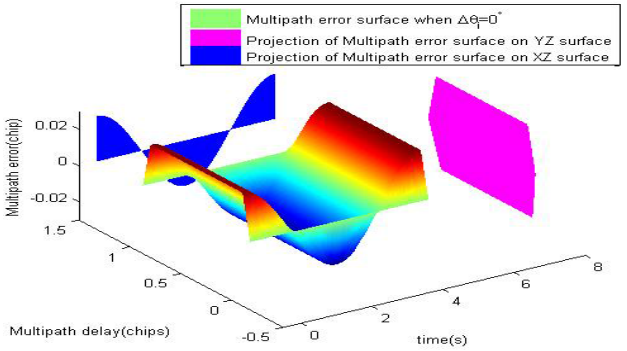

FIGURE 8. The surface of multipath error.

of code tracking loop. Therefore, the time-variant characteristics of multipath errors are the most significant difference between the multipath-Doppler and the normal multipath in code tracking.

IV. MULTIPATH-DOPPLER MITIGATION FRAMEWORK

As mentioned in Section 3, multipath-Doppler in the RF relative measurement exhibits unique time-variant characteristics. For this reason, the existing multipath mitigation methods based on estimation of multipath parameters do not work effectively in the presence of the multipath-Doppler (the analysis results are shown in Fig.14). In addition, it is very noteworthy that most of the existing methods consider the multipath signals as undesirable signals and always remove them from the received signal. On the basis of analyzing the disadvantages of the existing methods, a framework which can both effectively mitigate the multipath error and enhance the direct signal is proposed in the presence of multipath-Doppler. Moreover, in the case of only multipath exists, the proposed framework is still valid to mitigate multipath.

As shown in Fig.9, the proposed framework incorporates three essential parts: the parameters estimator, the reference signal generator and the signal reconstructor. The followings are the functions of each part of the proposed framework.

1) The parameter estimator is the core of the framework, and its function is to estimate the multipath and Doppler parameters (relative amplitude coefficient α_i, relative time-delay l_i, etc.) of the received signal.

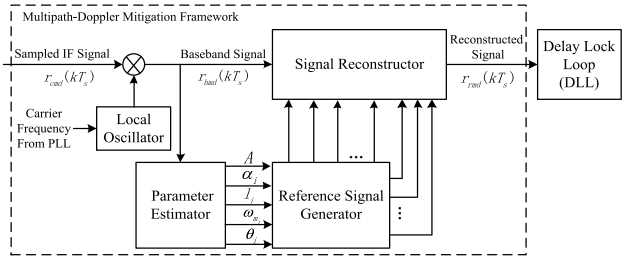

FIGURE 9. The multipath-doppler mitigation framework.

2) The function of reference signal generator is to generate the desired reference signals for the signal reconstructor, based on the estimated parameters from the parameter estimator.
3) The signal reconstructor reconstructs the received signal utilizing the locally generated reference signals to correct the distortion of received signal's correlation function, and the peak value of correction function is increased. Once this process is complete, the reconstructed signal is input to a DLL.

In the rest of this section, a detailed introduction of the theory and design of multipath-Doppler mitigation framework will be conducted from two aspects: estimation of multipath-Doppler and reconstruction of signal.

A. ESTIMATION OF MULTIPATH-DOPPLER PARAMETERS

In the proposed framework, to achieve the optimal signal reconstruction result, the reference signals generated by the reference signal generator need correspond to the multipath-Doppler characteristics of the received signal. Thus, before generating the reference signals, precise estimation of multipath-Doppler parameters of received signal should be obtained by the proposed parameter estimator. The structure of parameter estimator is shown in Fig.10.

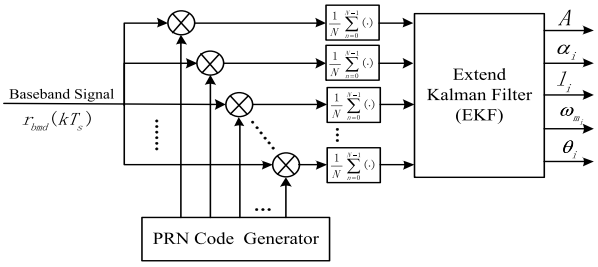

FIGURE 10. Multipath-doppler parameters estimator.

Assuming that the frequency and phase of locally generated carrier are the same as those of direct signal, the baseband signal obtained by the down conversion of sampled IF signal in the presence of multipath-Doppler can be expressed as:

$$\begin{aligned} r_{bmd}(kT_s) = {} & Ac(kT_s-\varepsilon) \\ & +A\sum_{i=1}^{N}\alpha_i c(kT_s-\varepsilon+l_i)\cos(-\mathrm{V}\omega_{m_i}kT_s+\theta_i) \\ & +n(kT_s) \end{aligned} \tag{22}$$

Due to the shape of correlation function can reflect the characteristics of the received signal. Thus, after down conversion, the baseband signal is correlated with a number of correlators to get samples of the correlation function. In an estimator, the locally generated PRN code corresponding to the n-th correlator is given by:

$$S_{I_n}(kT_s) = c(kT_s-\hat{\varepsilon}-\eta_n) \tag{23}$$

where η_n is the spacing in chips between the code delay of the local PRN code corresponding to the n-th correlator and the estimation of the direct signal code delay. Then, the correlation value output by the n-th correlator can be expressed as:

$$\begin{aligned} I_{e_n}(kT_s) = {} & \sum_{k=k_{0,j}}^{k_{0,j}+N-1} r_{bmd}(kT_s)S_{I_n}(kT_s) \\ \approx {} & \frac{AT_j}{2T_s}R(\mathrm{V}\varepsilon-\eta_n) \\ & +\frac{AT_j}{2T_s}\sum_{i=1}^{N}R(\mathrm{V}\varepsilon-\eta_n+l_i)\cos(\mathrm{V}\phi_{i,j}) \end{aligned} \tag{24}$$

where $\mathrm{V}\phi_{i,j} = -\mathrm{V}\omega_{m_i}(T_{0,j}+T_j/2)+\mathrm{V}\theta_i$.

The estimator estimates the amplitude (A) and code delay ($\mathrm{V}\varepsilon$) of the direct signal, as well as the relative amplitude coefficient (α_i), relative code delay (l_i), relative Doppler shift ($\mathrm{V}\omega_{m_i}$) and relative carrier phase ($\mathrm{V}\theta_i$) of each multipath signal. According to the number of parameters need to be estimated, the estimator requires two correlators for the direct signal and four correlators for each multipath signal. In practice, it is very rare that there are more than two dominant multipath signals present at one time. Thus, in normal operation, the estimator is configured to contain ten correlators to solve for the received signal consisting of direct signal and two multipath signals.

In this case, the matrices and vectors of the EKF estimator can be configured. The k-th state vector can be expressed as:

$$X_k = \left[A_k \mathrm{V}\varepsilon_k \alpha_{1,k} l_{1,k} \mathrm{V}\phi_{1,k} \mathrm{V}\omega_{m_1,k} \alpha_{2,k} l_{2,k} \mathrm{V}\phi_{2,k}\ \mathrm{V}\omega_{m_2,k}\right]^T \tag{25}$$

Thence, the state transition matrix is defined as:

$$F = \begin{bmatrix} 1 & 0 & 0 & 0 & 0 & 0 & 0 & 0 & 0 & 0 \\ 0 & 1 & 0 & 0 & 0 & 0 & 0 & 0 & 0 & 0 \\ 0 & 0 & 1 & 0 & 0 & 0 & 0 & 0 & 0 & 0 \\ 0 & 0 & 0 & 1 & 0 & 0 & 0 & 0 & 0 & 0 \\ 0 & 0 & 0 & 0 & 1 & T_j & 0 & 0 & 0 & 0 \\ 0 & 0 & 0 & 0 & 0 & 1 & 0 & 0 & 0 & 0 \\ 0 & 0 & 0 & 0 & 0 & 0 & 1 & 0 & 0 & 0 \\ 0 & 0 & 0 & 0 & 0 & 0 & 0 & 1 & 0 & 0 \\ 0 & 0 & 0 & 0 & 0 & 0 & 0 & 0 & 1 & T_j \\ 0 & 0 & 0 & 0 & 0 & 0 & 0 & 0 & 0 & 1 \end{bmatrix} \tag{26}$$

The measurement vector consisting of the correlation results obtained by 10 correlators can be expressed as:

$$Y_k = \left[I_{e_1,k} I_{e_2,k} I_{e_3,k} \cdots I_{e_{10},k}\right]^T \tag{27}$$

The Jacobian matrix (H) corresponding to the measurement functions (Eq. 22) can be derived as:

$$\left[\frac{\partial I_{e_i}}{\partial A_k}\ \frac{\partial I_{e_i}}{\partial \mathrm{V}\varepsilon_k}\ \frac{\partial I_{e_i}}{\partial \mathrm{V}\alpha_{1,k}}\ \frac{\partial I_{e_i}}{\partial l_{1,k}}\ \frac{\partial I_{e_i}}{\partial \mathrm{V}\phi_{1,k}}\ \frac{\partial I_{e_i}}{\partial \mathrm{V}\omega_{m_1,k}}\ \frac{\partial I_{e_i}}{\partial \mathrm{V}\alpha_{2,k}}\ \frac{\partial I_{e_i}}{\partial l_{2,k}}\ \frac{\partial I_{e_i}}{\partial \mathrm{V}\phi_{2,k}}\ \frac{\partial I_{e_i}}{\partial \mathrm{V}\omega_{m_2,k}}\right]^T \tag{28}$$

where $i = 1, 2, 3\mathrm{L}\ldots, 10$.

TABLE 1. Experiment scenario.

Experiments	Multipath	PRN code length (*chips*)	Rate of code (MHz)	SNR (dB)	A (V)	$V\varepsilon$ (*chips*)	α_1	l_1 (*chips*)	$V\omega_{m_1}$ (rad/s)	α_2	l_2 (*chips*)	$V\omega_{m_2}$ (rad/s)
Scenario1	2	1023	1.023	10	1	0.1	0.5	0.3	503	0.3	0.8	377
Scenario2	2	1023	1.023	-20-30	1	0.1	0.5	0.3	503	0.3	0.8	377
Scenario3	2	1023	1.023	10	1	0.1	0.5	0.3	503	0.3	0.8	377

Following the above configuration, the estimate of multipath and Doppler parameters can be obtained. Due to the proposed framework is valid in multipath and multipath-Doppler scenarios, and the EKF estimator is the core of the framework, it is necessary to verify its functionality in both scenarios. Experiments for both scenarios are presented and results are shown in Fig.13 and Fig.14, respectively. In the presence of multipath-Doppler, Fig.13 shows a part of parameters estimation result, and the simulation conditions is same as Scenario2 in Section 5, which are shown in Table 1.

As shown in Fig.11, all the estimated parameters have converged during the estimation process. Therefore, the accurate estimate of parameters of received signal can be obtained by the estimator, and the estimation precision of multipath-Doppler parameters can meet requirements of signal reconstruction.

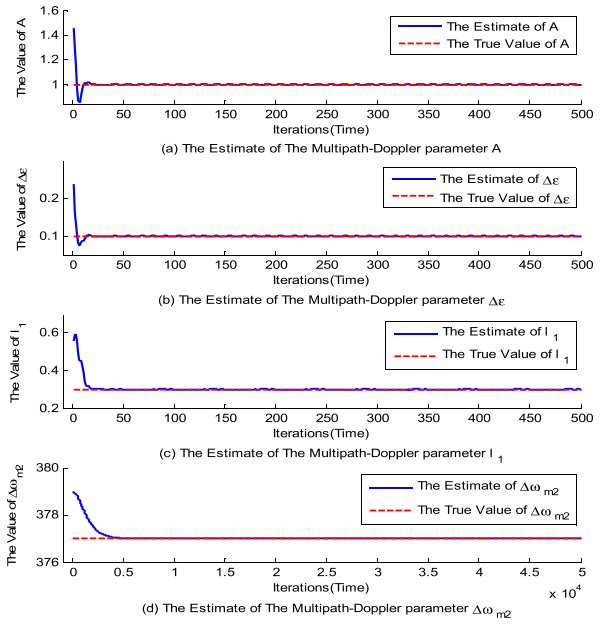

FIGURE 11. Estimate of multipath-doppler parameters.

In scenario where there is only multipath, $V\omega_{m_1}$ and $V\omega_{m_2}$ become zero, and other parameters are unchanged. Results of the estimation are shown in Fig.12.

It can be found from Fig.12 that all the estimated parameters have converged, and results are similar to the scenario

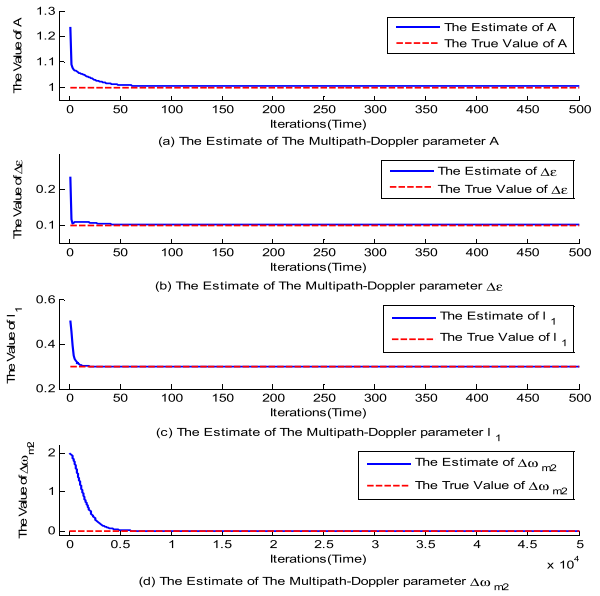

FIGURE 12. Estimate of multipath parameters.

with multipath-Doppler. Thence, the multipath-Doppler estimator is universal in both scenarios.

B. RECONSTRUCTION OF SIGNAL

After the estimates of parameters are obtained, the reference signal generator and the signal reconstructor begin to reconstruct the received signal utilizing the joint multipath-Doppler diversity to mitigate the multipath signal and enhance the direct signal. The structure of reference signal generator and signal reconstructor is shown in Fig.13.

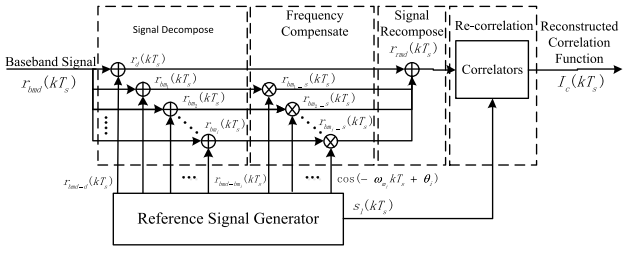

FIGURE 13. The structure of reference signal generator and reconstructor.

1) SIGNAL DECOMPOSE

The first step of the signal reconstruction is to decompose the received signal. Based on the estimated parameters obtained by the parameters estimator, the estimate of the direct signal and i-th multipath-Doppler signal can be expressed as follows, respectively:

$$\hat{r}_{bd}(kT_s) = \hat{A}c(kT_s - \hat{\varepsilon}) \tag{29}$$

$$\hat{r}_{bm_i}(kT_s) = \hat{A}\hat{a}_i c(kT_s - \hat{\varepsilon} - \hat{l}_i)\cos(-\mathrm{V}\hat{\omega}_{m_i}kT_s + \mathrm{V}\hat{\theta}_i) \tag{30}$$

where $\mathrm{V}\hat{\theta}_i = \mathrm{V}\hat{\phi}_{i,j} + \mathrm{V}\hat{\omega}_{m_i}(T_{0,j} + T_j/2)$.

Then, the direct signal can be obtained by subtracting the sum of the estimates of each multipath signal from the received signal as follows:

$$\begin{aligned} r_{bd}(kT_s) &= r_{bmd}(kT_s) - \hat{r}_{bmd-d}(kT_s) \\ &= r_{bmd}(kT_s) - \sum_{i=1}^{M} \hat{r}_{bm_i}(kT_s) \end{aligned} \tag{31}$$

The i-th multipath-Doppler signal is obtained by the similar method.

$$\begin{aligned} r_{bm_i}(kT_s) &= r_{bmd}(kT_s) - \hat{r}_{bmd-bm_i}(kT_s) \\ &= r_{bmd}(kT_s) - \hat{r}_d(kT_s) - \sum_{\substack{m=1 \\ m\neq i}}^{M} \hat{r}_{bm_m}(kT_s) \end{aligned} \tag{32}$$

2) FREQUENCY COMPENSATE

Due to multipath-Doppler has the time-varying characteristic, in some cases the direct signal can be weakened. Therefore, Frequency compensation is proposed in this study to maintain the positive of correlation function of the signal in any case. Method as [15] pointed out does not consider the time-varying characteristic, and in some cases the direct signal is weakened. Therefore, this step is to multiply the i-th multipath-Doppler signal by the estimate of its residual carrier as Eq.(33).

$$\begin{aligned} r_{bm_i\_s}(kT_s) &= r_{bm_i}(kT_s)\cdot\cos(-\mathrm{V}\omega_{m_i}kT_s + \mathrm{V}\theta_i) \\ &= Aa_i c(kT_s - \varepsilon - l_i)\cos(-\mathrm{V}\omega_{m_i}kT_s + \mathrm{V}\theta_i)^2 \end{aligned} \tag{33}$$

3) SIGNAL RECOMPOSE

In the third step, the direct signal and frequency-compensated multipath-Doppler signal are re-composed to obtain the desired reconstructed signal as follows:

$$\begin{aligned} r_{rmd}(kT_s) &= r_{bd}(kT_s) + \sum_{i=1}^{M} r_{bm_i\_s}(kT_s) \\ &= Ac(kT_s - \varepsilon) \\ &\quad + \sum_{i=1}^{M} Aa_i c(kT_s - \varepsilon - l_i)\cos(-\mathrm{V}\omega_{m_i}kT_s + \mathrm{V}\theta_i)^2 \end{aligned} \tag{34}$$

4) RE-CORRELATION

After obtaining the reconstructed signal, the signal reconstructor correlates the reconstructed signal and local generated reference signal utilizing a similar set of correlators as in the parameters estimator. The reference signal generated by the reference signal generator corresponding to n-th correlator is as follows:

$$\begin{aligned} &s_{l_n}(kT_s) \\ &= s_{bd_n}(kT_s) + \sum_{i=1}^{M} s_{bm_i\_s_n}(kT_s) \\ &= Ac(kT_s - \hat{\varepsilon} - \eta_n) \\ &\quad + A\sum_{i=1}^{M} \alpha_i c(kT_s - \hat{\varepsilon} - l_i - \eta_n)\cos(-\mathrm{V}\omega_{m_i}kT_s + \mathrm{V}\theta_i)^2 \end{aligned} \tag{35}$$

Then, the correlation value output by the n-th correlator can be expressed as:

$$\begin{aligned} I_{c_n}(kT_s) &= \sum_{k=k_{0,j}}^{k_{0,j}+N-1} r_{rmd}(kT_s)s_{l_n}(kT_s) \\ &= I_{r_n,d}(kT_s) + I_{r_n,m}(kT_s) + I_{r_n,l}(kT_s) + I_{r_n,r}(kT_s) \end{aligned} \tag{36}$$

As shown in Eq.36 the correlation value consists of two square terms ($I_{c_n,d}(kT_s)$, $I_{c_n,m}(kT_s)$) and two cross terms ($I_{c_n,l}(kT_s)$, $I_{c_n,r}(kT_s)$). In addition, each term can be derived as A1-A4 in Appendix.

Figure 14 shows the correlation function of the reconstructed signal and reference signal, and the simulation conditions is same as Scenario 3 in Section 5, which are shown in Table 1.

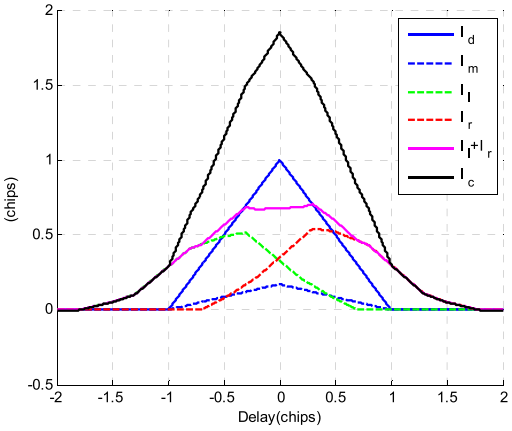

FIGURE 14. The curve of the correlation function.

It can be shown from Fig.14 that the curves of both square terms ($I_{c,d}$, $I_{c,m}$) are symmetrical and the center of symmetry is $\mathrm{V}\varepsilon = 0$. The sum of curves corresponding to two cross terms ($I_{c,l}$, $I_{c,r}$) is also symmetric around $\mathrm{V}\varepsilon = 0$. Thus, the curve of correlation function (I_c) consisting of $I_{c,d}$, $I_{c,m}$, $I_{c,l}$ and $I_{c,r}$ is symmetrical, this means that the multipath error is reduced [18].

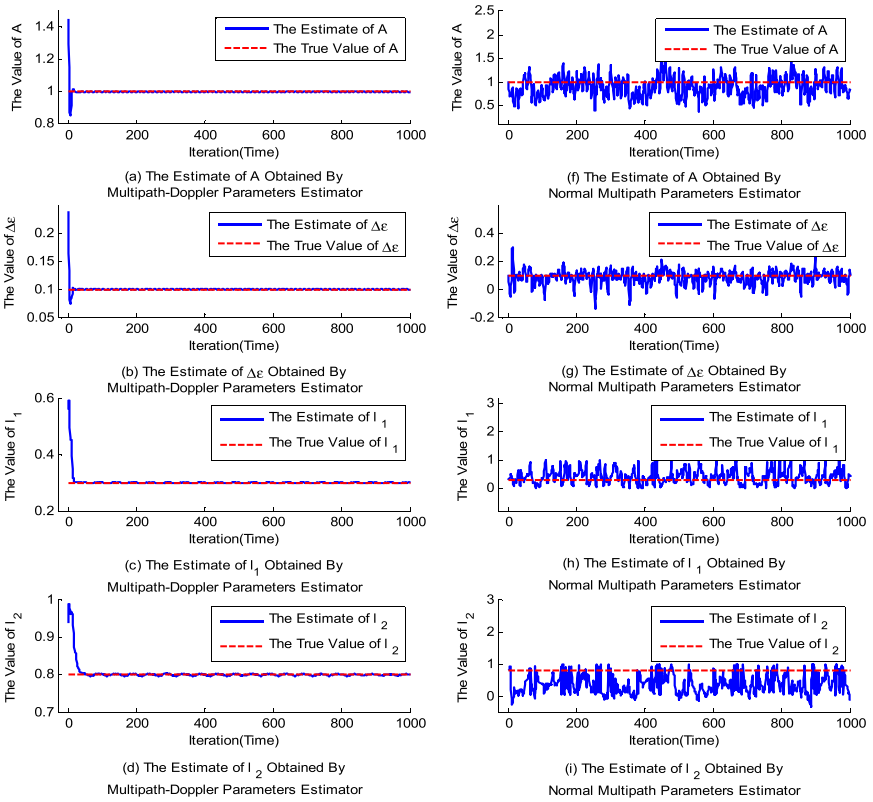

FIGURE 15. Comparison of proposed estimator and normal multipath estimator.

It is also worth noting that, the height of the correlation peak of the reconstructed signal (the black line) is higher than that of the direct signal (the blue line), indicating that the direct signal is enhanced.

Therefore, the following conclusions can be drawn: when the multipath-Doppler effect occurs, the proposed framework can mitigate the multipath error, and enhance the direct signal.

V. EXPERIMENTS AND RESULTS

A. TEST OF MULTIPATH ESTIMATION

To verify the performance of the proposed framework of multipath mitigation, a simulation experiment was designed consisting of three experimental scenarios.

In Scenario 1, the performance of multipath-Doppler estimators and normal multipath estimators is compared in the presence of multipath and Doppler.

In Scenario 2, to verify the estimation performance of the proposed EKF estimator in noisy environment, the root mean square error (RMSE) of the estimated parameters under different signal to noise ratios (SNR) is calculated and recorded.

In addition, to verify the multipath mitigation performance after signal reconstruction, we thus designed Scenario 3. In Scenario 3 the proposed signal reconstructor and that in the existing method are compared, with respect to the correlation function and discriminator function, respectively. Details of the three experimental scenarios are listed in Table 1.

B. RESULTS OF SCENARIO 1

Figure 15 shows a part of estimation results of experimental Scenario 1. The following was observed:

1) In the presence of multipath and Doppler, the estimated parameters of the multipath-Doppler estimator, which are shown in the left part of Fig.15, converged. In contrast, those of the normal Doppler estimator, which are shown in the right part of Fig.15, do not converge and the estimation errors are large.

2) In contrast, multipath-Doppler estimator has commonality in multipath-Doppler scenario and multipath scenario; whereas, the normal multipath estimator do not operate in the presence of multipath and Doppler. This is due to the proposed estimator takes into account the unique time-variant characteristic of multipath error, and takes $V\omega_m$ which reflects the time-variant characteristic as a parameter to be estimated.

C. RESULTS OF SCENARIO 2

The experimental results of Scenario 2 are given in Fig.16. From them, the following should be noted:

1) The RMSE of the estimated parameters (in logarithmic form) is linearly related to the SNR of the received signal, and it decreases with the increase of the SNR. This shows that the SNR is the main factor that affects the estimation accuracy of the proposed parameters estimator.

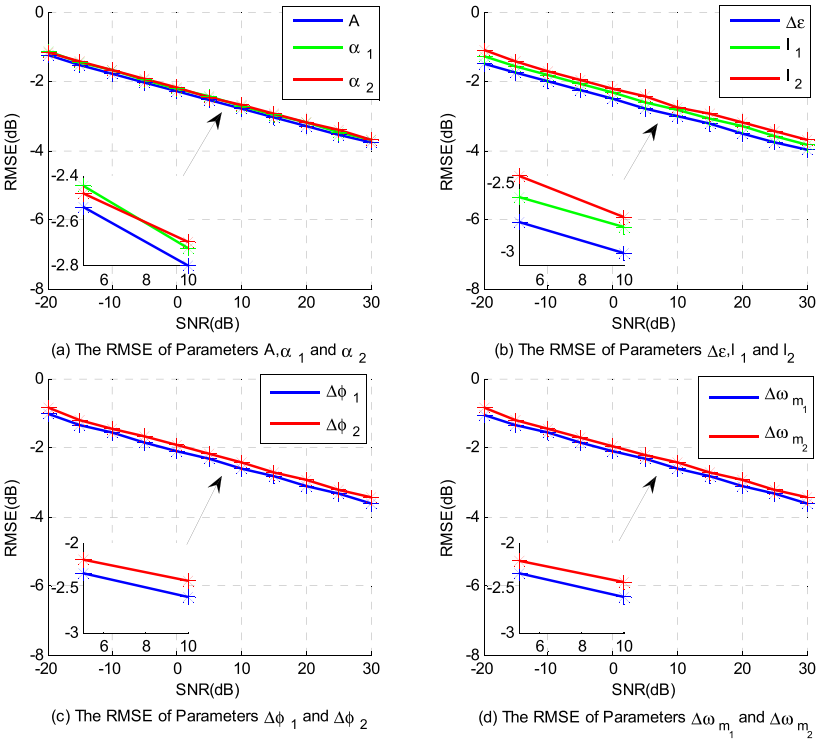

FIGURE 16. The performance of estimator at different SNR.

2) In the case of lower signal-to-noise ratio, such as SNR $= -20$dB, the estimator still work normally, which means that the estimator has the strong capability of noise immunity, and can satisfy the actual application requirements.

D. RESULTS OF SCENARIO 3

From Section 5.3, it is evident that the estimation performance of proposed EKF estimator can satisfy performance requirements of the reconstructor. Thence, the received multipath-Doppler signal can be reconstructed based on the joint multipath Doppler diversity, and the reconstruction result can be expressed from the correlation function and discriminator curve. Therefore, the tracking performance of the method in [15] and the proposed method are compared. Figure 17 shows the results of Scenario 3, from which the following is evident:

1) From the symmetry of the correlation function (Fig.17 (a) and (b)) and the position of the zero crossing of the discriminator curve (Fig.17 (c) and (d)), it can be found that the both methods can mitigate multipath.

2) However, by comparing (a) and (b), it can be found that the peak value of the correlation function is increased with the proposed method; whereas, method as [15] pointed out direct signal strength is reduced in some cases, and Scenario 3 is one of cases. Due to the proposed method takes into account the time-varying characteristics of multipath-Doppler.

3) By comparing (c) and (d), the slope of discriminator curve with the proposed method is improved, due to the direct signal is enhanced. For this reason, the performance of the discriminator is effectively improved.

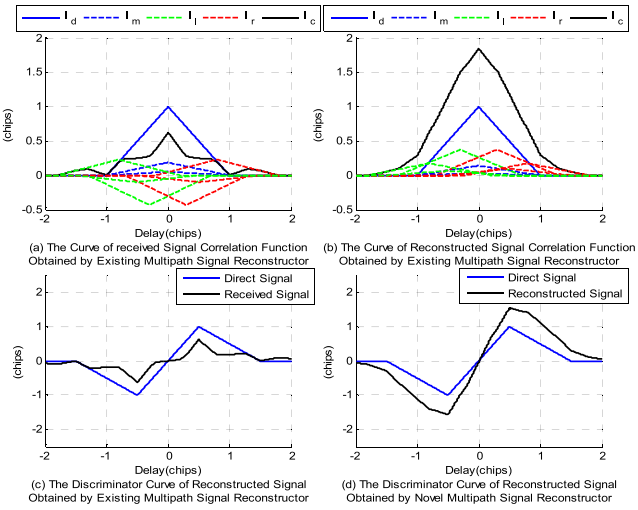

FIGURE 17. The multipath mitigation performance comparison.

VI. CONCLUSION

1) This study presents a multipath mitigation framework which is suitable for multipath and multipath-Doppler scenarios. In this framework, multipath and Doppler parameters can be accurately estimated by the EKF multipath estimator; the signal reconstructor can effectively increase the signal strength by using joint multipath Doppler diversity.

2) The performance of the proposed framework and its estimator and reconstructor are validated experimentally. Compared with existing methods, the performance of multipath mitigation is improved in present of multipath and Doppler.

APPENDIX

$$
\begin{aligned}
&I_{c_n,d}(kT_s)\\
&=\sum_{k=k_{0,j}}^{k_{0,j}+N-1} r_{bd}(kT_s)s_{bd_n}(kT_s)\\
&=\sum_{k=k_{0,j}}^{k_{0,j}+N-1} A^2c(kT_s-\varepsilon)c(kT_s-\hat{\varepsilon}-\eta_n)\\
&=A^2R(\mathrm{V}\varepsilon-\eta_n) \qquad \text{(A1)}\\
&I_{c_n,m}(kT_s)\\
&=\sum_{i=1}^{M}\sum_{k=k_{0,j}}^{k_{0,j}+N-1} r_{bm_{i\_}s}(kT_s)s_{bm_{i\_}s_n}(kT_s)\\
&=\sum_{i=1}^{M}\sum_{k=k_{0,j}}^{k_{0,j}+N-1} [A^2\alpha_i^2c(kT_s-\varepsilon-l_i)\cos(-\mathrm{V}\omega_{m_i}kT_s+\mathrm{V}\theta_i)^2\\
&\quad\cdot c(kT_s-\hat{\varepsilon}-l_i-\eta_n)\cos(-\mathrm{V}\omega_{m_i}kT_s+\mathrm{V}\theta_i)^2]\\
&\approx\sum_{i=1}^{M}A^2\alpha_i^2R(\mathrm{V}\varepsilon-\eta_n)(\frac{3}{8}+\frac{1}{2}\cos(2\mathrm{V}\phi_{i,j})+\frac{1}{8}\cos(4\mathrm{V}\phi_{i,j}))
\end{aligned}
\qquad \text{(A2)}
$$

$$
\begin{aligned}
&I_{c_n,r}(kT_s)\\
&=\sum_{i=1}^{M-1}\sum_{m=i+1}^{M} r_{bm_{i\_}s}(kT_s)s_{bm_{m\_}s_n}(kT_s)\\
&=\sum_{i=1}^{M-1}\sum_{m=i+1}^{M}\sum_{k=k_{0,j}}^{k_{0,j}+N-1} [A^2\alpha_i\alpha_mc(kT_s-\varepsilon-l_i)\cos(-\mathrm{V}\omega_{m_i}kT_s+\mathrm{V}\theta_i)^2\\
&\quad\cdot c(kT_s-\hat{\varepsilon}-l_m-\eta_n)\cos(-\mathrm{V}\omega_{m_m}kT_s+\mathrm{V}\theta_m)^2]\\
&\approx\sum_{i=1}^{M-1}\sum_{m=i+1}^{M} [A^2\alpha_i\alpha_mR(\mathrm{V}\varepsilon+l_i-l_m-\eta_n)\cdot(\frac{1}{4}+\frac{1}{4}\cos(\mathrm{V}\phi_{i,j})\\
&\quad+\frac{1}{4}\cos(\mathrm{V}\phi_{m,j})+\frac{1}{8}\cos(\mathrm{V}\phi_{i,j}+\mathrm{V}\phi_{m,j})\\
&\quad+\frac{1}{8}\cos(\mathrm{V}\phi_{i,j}-\mathrm{V}\phi_{m,j}))] \qquad \text{(A3)}\\
&I_{c_n,l}(kT_s)\\
&=\sum_{i=2}^{M}\sum_{m=1}^{i-1} r_{bm_{i\_}s}(kT_s)s_{bm_{m\_}s_n}(kT_s)\\
&=\sum_{i=2}^{M}\sum_{m=1}^{i-1}\sum_{k=k_{0,j}}^{k_{0,j}+N-1} [A^2\alpha_i\alpha_mc(kT_s-\varepsilon-l_i)\cos(-\mathrm{V}\omega_{m_i}kT_s+\mathrm{V}\theta_i)^2\\
&\quad\cdot c(kT_s-\hat{\varepsilon}-l_m-\eta_n)\cos(-\mathrm{V}\omega_{m_m}kT_s+\mathrm{V}\theta_m)^2]\\
&\approx\sum_{i=2}^{M}\sum_{m=1}^{i-1} [A^2\alpha_i\alpha_mR(\mathrm{V}\varepsilon+l_i-l_m-\eta_n)\cdot(\frac{1}{4}+\frac{1}{4}\cos(\mathrm{V}\phi_{i,j})\\
&\quad+\frac{1}{4}\cos(\mathrm{V}\phi_{m,j})+\frac{1}{8}\cos(\mathrm{V}\phi_{i,j}+\phi_{m,j})\\
&\quad+\frac{1}{8}\cos(\mathrm{V}\phi_{i,j}-\mathrm{V}\phi_{m,j}))] \qquad \text{(A4)}
\end{aligned}
$$

REFERENCES

[1] D'Errico and E. Marco, *Distributed Space Missions for Earth System Monitoring*, vol. 31. New York, NY, USA: Springer, 2012, pp. 945–948.
[2] B. Z. Urioste, A. Naseri, S. Stochaj, N. Shah, and J. Krizmanic, "Relative navigation schemes for formation flying of satellites," in *Proc. Small Satell. Conf. Big Picture*, 2017. [Online]. Available: http://digitalcommons.usu.edu/smallsat/2017/all2017/29/
[3] P. Bodin, R. Noteborn, R. Larsson, T. Karlsson, S. D'Amico, J. S. Ardaens, M. Delpech, and J. C. Berges, "The prisma formation flying demonstrator: Overview and conclusions from the nominal mission," *Adv. Astron. Sci.*, vol. 144, pp. 441–460, Feb. 2012.
[4] E. Gill, P. Sundaramoorthy, J. Bouwmeester, B. Zandbergen, and R. Reinhard, "Formation flying within a constellation of nano-satellites: The QB50 mission," *Acta Astronautica*, vol. 82, no. 1, pp. 110–117, Jan. 2013.
[5] S. Bandyopadhyay, R. Foust, G. P. Subramanian, S.-J. Chung, and F. Y. Hadaegh, "Review of formation flying and constellation missions using nanosatellites," *J. Spacecraft Rockets*, vol. 53, no. 3, pp. 567–578, May 2016.
[6] M. Aung, G. H. Purcell, J. Y. Tien, L. E. Young, L. R. Amaro, J. Srinivan, M. A. Ciminera, and Y. J. Chong, "Autonomous formation flying sensor for the starlight mission," in *Proc. Int. Symp. Formation Flying Missions Technol.*, Toulouse, France, Oct. 2002.
[7] M. Delpech, J. C. Berges, T. Karlsson, and F. Malbet, "Results of PRISMA/FFIORD extended mission and applicability to future formation flying and active debris removal missions," *Int. J. Space Sci. Eng.*, vol. 4, no. 2, pp. 382–409, 2013.
[8] M. Powe, F. Zanier, M. Porretta, A. Garcia-Rodriguez, and O. Mongrard, "Analysis of the international space station multipath and masking environment for automated transfer vehicle relative GPS rendezvous manoeuvres," in *Proc. 6th ESA Workshop Satell. Navigat. Technol. (Navitec) Eur. Workshop GNSS Signals Signal Process.*, Dec. 2012, pp. 1–7.
[9] K. Zhang and F. Wang, "Joint code multipath mitigation for composite binary offset carrier modulated signals," *Electron. Lett.*, vol. 47, no. 25, pp. 1374–1375, Dec. 2011.
[10] Z. Liu, L. Huang, X. Tang, and F. Wang, "Multipath mitigation strobe for global navigation satellite system receivers," *Electron. Lett.*, vol. 11, pp. 962–963, May 2016.
[11] P. C. Fenton and J. Jones, "The theory and performance of NovAtel Inc.'s vision correlator," in *Proc. ION GNSS*, 2005, pp. 2178–2186.
[12] J. K. Ray, *Mitigation of GPS Code and Carrier Phase Multipath Using a Multi-Antenna System*. Calgary, AB, Canada: Univ. Calgary, 2000.
[13] M. Irsigler, *Multipath Propagation, Mitigation and Monitoring in the Light of Galileo and the Modernized GPS*. Neubiberg, Germany: Universität der Bundeswehr München, 2008.
[14] A. Giremus, J.-Y. Tourneret, and V. Calmettes, "A particle filtering approach for joint detection/estimation of multipath effects on GPS measurements," *IEEE Trans. Signal Process.*, vol. 55, no. 4, pp. 1275–1285, Apr. 2007.
[15] F. Xiang, G. Liao, C. Zeng, and W. Wang, "A multipath mitigation discriminator for GPS receiver," *AEU Int. J. Electron. Commun.*, vol. 67, no. 10, pp. 839–847, Oct. 2013.
[16] B. W. Ashman, J. L. Veldman, P. Axelrad, J. L. Garrison, and L. B. Winternitz, "Validation of GNSS multipath model for space proximity operations using the hubble servicing mission 4 experiment," in *Proc. 29th Int. Tech. Meeting Satell. Division Inst. Navigat. (ION GNSS+)*, Nov. 2016, pp. 1–9.

[17] P. Xie, M. G. Petovello, and C. Basnayake, "Multipath signal assessment in the high sensitivity receivers for vehicular applications," in *Proc. ION GNSS*, 2011, pp. 1764–1776.
[18] R. Sun, *Relative Navigation for Satellite Formation Flying Based on Radio Frequency Metrology*. Delft, The Netherlands: Delft Univ. Technology, 2014.
[19] J. Lesouple, T. Robert, M. Sahmoudi, J.-Y. Tourneret, and W. Vigneau, "Multipath mitigation for GNSS positioning in an urban environment using sparse estimation," *IEEE Trans. Intell. Transp. Syst.*, vol. 20, no. 4, pp. 1316–1328, Apr. 2019.
[20] A. Kumar and A. K. Singh, "A novel multipath mitigation technique for GNSS signals in urban scenarios," *IEEE Trans. Veh. Technol.*, vol. 69, no. 3, pp. 2649–2658, Mar. 2020.

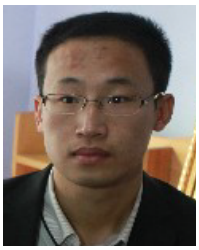

WEIQING MU received the Ph.D. degree in communication and information engineering from Beihang University, in 2018. He is currently with the Postdoctoral Workstation, China Research Institute of Radiowave Propagation. His current research interests include spectrum monitoring, dynamic frequency sharing, and radio frequency relative measurement.

ZIJIE WANG received the B.S. degree in electrical and information engineering from Beihang University, China, in 2017, where he is currently pursuing the Ph.D. degree with the School of Electronic and Information Engineering. His current research interests include global navigation satellite systems, terrestrial localization systems, indoor/outdoor seamless positioning, unmanned aerial vehicles, and applications of these technologies to 5G and the Internet of Things networks.

LANTU GUO is currently pursuing the Ph.D. degree with the School of Information and Electronics, Beijing Institute of Technology, Beijing, China. His current research interests include passive positioning and spectrum monitoring.

YANAN LIU is currently pursuing the Ph.D. degree with the School of Information and Communication Engineering, Harbin Engineering University, Harbin, China. His current research interests include passive positioning and the Internet of Things networks.